Journal of Zhejiang University-SCIENCE A (Applied Physics & Engineering) in press
www.jzus.zju.edu.cn; www.springer.com/journal/11582
E-mail: jzus_a@zju.edu.cn

Correspondence

https://doi.org/10.1631/jzus.A2300514

Monotonic mechanical behaviour of compacted completely decomposed granite with various inclusion levels of incineration bottom ash

Han-Lin WANG[1,2,3], Cheng-Shuang YIN[1,2,3], Qian-Yi ZHANG[4], Qi-Wei LIU[1,2,3]✉, Zhen-Yu YIN[5]✉, Dong-Xing XUAN[5]

[1]*Research Center for Advanced Underground Space Technologies of Hunan University, Changsha 410082, China*
[2]*Key Laboratory of Building Safety and Energy Efficiency of the Ministry of Education, Hunan University, Changsha 410082, China*
[3]*College of Civil Engineering, Hunan University, Changsha 410082, China*
[4]*School of Civil Engineering, Zhengzhou University, Zhengzhou 450001, China*
[5]*Department of Civil and Environmental Engineering, The Hong Kong Polytechnic University, Hung Hom, Kowloon, Hong Kong, China*

Unedited

1 Introduction

Completely decomposed granite (CDG) is widely distributed in South China (Xu et al., 2022; Wang et al., 2023). The parent granite rock mass gradually loses features during the weathering process, and thus needs to be reinforced when used (Lan et al., 2003; Dassekpo et al., 2017; Alamanis et al., 2021). On the other hand, considering the huge demand for construction materials and limited natural resources, it is increasingly important to fully utilize solid waste (Gruhler et al., 2019; Anagnostopoulos et al., 2020; Jiang et al., 2022, 2023a, 2023b). With high strength and environment-friendly characteristics, incineration bottom ash (IBA) seems to be a suitable reinforcement material for CDG (Ahmed and Khalid, 2011; Alhassan and Tankó, 2012; Toraldo et al., 2013; Lynn et al., 2017; Xuan et al., 2018; Tang et al., 2020). Both reinforcement and environmental issues should be addressed when considering treatment of CDG with IBA.

To date, investigations of soil treatment with IBA have been widely reported. For example, Gupta et al. (2021) showed that IBA has better shear resistance and compressibility behaviour than soft soils. When IBA content is increased from 10% to 30%, the unconfined compressive strength of the expansive soil-IBA mixture significantly increases (Melese, 2022; Randhawa et al., 2022). However, the effect of the compaction degree of the matrix soil was not considered in most previous studies, although it was a significant indicator for soil reinforcement. Furthermore, the mechanism by which IBA reinforces soil has not yet been comprehensively interpreted.

To evaluate the feasibility of applying IBA for soil reinforcement, we examined the monotonic mechanical behaviour of a CDG-IBA mixture by a series of monotonic triaxial tests. Various volumetric amounts of IBA were added to the CDG, followed by compaction to different compaction degrees. The monotonic mechanical behaviours of the samples were analysed from the testing results. The investigation revealed the strengthening mechanism of the IBA in the compacted mixture.

2 Materials and methods

2.1 Testing materials

The natural CDG soil was extracted from a highway construction site in Tai Wai, Hong Kong, China (Xu et al., 2022; Wang et al., 2023). It was

---

✉ Qi-Wei LIU, liuqw@hnu.edu.cn
Zhen-Yu YIN, zhenyu.yin@polyu.edu.hk
Zhen-Yu YIN, https://orcid.org/0000-0003-4154-7304

Received Oct. 10, 2023; Revision accepted Dec. 14, 2023; Crosschecked

© Zhejiang University Press 2024

Unedited

grinded and passed through a 2-mm sieve for testing. The grain-size distribution curve is shown in Fig. 1. The main minerals contained in the CDG were quartz, albite, illite, kaolinite, calcite, and muscovite, according to the X-ray diffraction (XRD) test. The main chemical components were obtained by X-ray fluorescence (XRF), and were found to be SiO_2 (61.12%) and Al_2O_3 (30.19%). The specific gravity G_s of the CDG was 2.59. The content of particles smaller than 0.075 mm was 54%, and the plastic limit and liquid limit were 15.3% and 33.5%, respectively. The soil could be classified as lean clay (CL; ASTM 2017). We conducted the standard Proctor compaction test (ASTM 2012), and the result is shown in Fig. 2. The optimum water content $w_{\text{opt-C}}$ was 14.5% and the maximum dry density $\rho_{d\max-C}$ was 1.83 Mg/m^3.

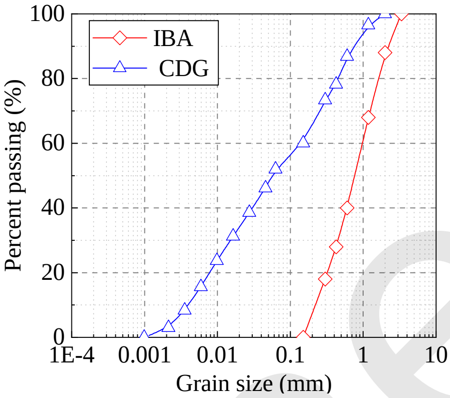

Fig. 1 Grain size distribution curves of CDG and IBA

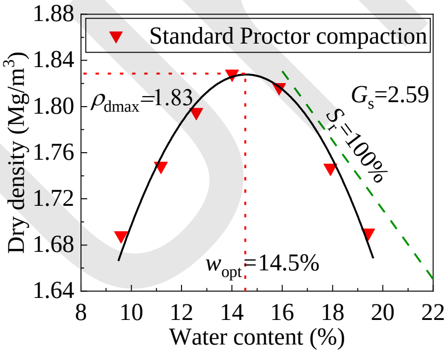

Fig. 2 Compaction curve of CDG

The IBA was collected from a waste-to-energy plant in Hang Zhou, China (Xuan et al., 2018; Tang et al., 2020). IBA particles ranging from 0.1 mm to 2 mm were used after screening and crushing cycles; the particle-size distribution is shown in Fig 1. IBA is a coarse-grained material with a rough surface texture, porous microstructure, and irregularly shaped particles. The IBA particles in this study primarily consisted of quartz and calcite, as determined by an XRD test (Lynn et al., 2017). The chemical components of IBA are relatively inactive, with a negligible effect on the physical properties of soil. The dry unit mass of IBA $\rho_{\text{s-I}}$ was 2.60 Mg/m^3.

2.2 Definition of volumetric content of IBA

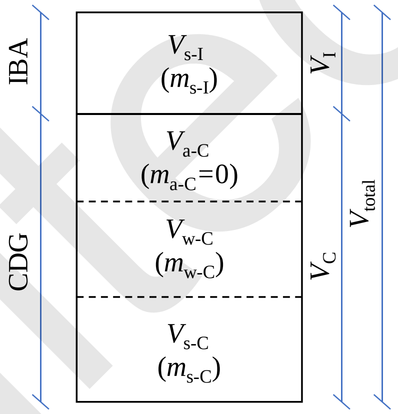

Fig. 3 Definition for soil constituents

To quantify the composition and clearly illustrate the soil structure, we introduced the volumetric content of IBA f_v (Fig. 3), representing the ratio of the IBA particle volume V_I to the total volume of the sample V_{total} (Seif El Dine et al., 2010; Wang et al., 2017, 2018a, 2018b):

$$f_v = \frac{V_I}{V_{\text{total}}} \tag{1}$$

To better demonstrate the volumetric content of IBA particles (see Fig. 3), it is assumed that air and water only exist in the CDG soil, while the IBA contains only solid particles (following the definitions from Wang et al., 2018a). The chemical activity of the IBA is relatively stable, with negligible chemical effects on soil strength. The total volume of the sample V_{total} can be calculated by the size of the sample (diameter: 50 mm; height: 100 mm). If f_v is given, the V_I can be determined accordingly using Eq. (1).

Unedited

Using $\rho_{\text{s-I}} = 2.60\ \text{Mg/m}^3$, the mass of the IBA $m_{\text{s-I}}$ can be obtained as:

$$m_{\text{s-I}} = \rho_{\text{s-I}} V_{\text{I}} \tag{2}$$

As shown in Fig. 3, the volume V_{C} of the CDG can be calculated as:

$$V_{\text{C}} = V_{\text{total}} - V_{\text{I}} = V_{\text{s-C}} + V_{\text{a-C}} + V_{\text{w-C}} \tag{3}$$

where $V_{\text{s-C}}$, $V_{\text{w-C}}$, and $V_{\text{a-C}}$ are the volumes of soil solids, water, and air in CDG, respectively.

During sample preparation, the water content of the CDG was controlled to the optimum water content $w_{\text{opt-C}}$. Three compaction degrees D_{C} of the CDG were adopted to the values used by Chen et al. (2019), defined as the ratio of the dry density of the CDG to its maximum dry density. Using the compaction parameters, the mass of the solid $m_{\text{s-C}}$ and water $m_{\text{w-C}}$ in the CDG can be determined as:

$$m_{\text{s-C}} = \rho_{\text{dmax-C}} D_{\text{C}} V_{\text{C}} \tag{4}$$

$$m_{\text{w-C}} = m_{\text{s-C}} w_{\text{opt-C}} \tag{5}$$

2.3 Testing procedures

We selected different values for the volumetric contents of IBA, as listed in Table 1. For sample preparation, we mixed the oven-dried CDG soil with water to achieve its optimum water content $w_{\text{opt-C}}$. The mixed soil was stored in a sealed container for 24 hours for moisture homogenization. Then, the soil was mixed with predetermined masses of dry IBA particles, followed by uniform compaction in a mould in three layers to achieve the target compaction degree of the CDG (see Table 1).

After sample preparation, monotonic triaxial tests were conducted with the drainage valve open and an axial shear rate of 0.1 mm/min (following Wang et al., 2018a). No saturation program was applied after mounting the samples, so that all samples remained unsaturated during the test. The tests were terminated when the axial strain of samples reached 18%, at which point they were considered to have entered the ultimate state.

Table 1 Basic and mechanical properties of samples

Sample	D_{c} (%)	f_{v} (%)	$w_{\text{opt-C}}$ (%)	$\rho_{\text{dmax-C}}$ (Mg/m^3)	$S_{\text{r-C}}$ (%)	$m_{\text{s-C}}$ (g)	$m_{\text{s-I}}$ (g)	e	c_{ps} (kPa)	φ_{ps} (°)
I	85	0	14.5	1.83	56.5	305.4	0	0.66	46.7	23.4
II	85	10	14.5	1.83		274.9	51.1	0.59	62.4	29.3
III	85	20	14.5	1.83		244.3	102.2	0.53	94.7	32.7
IV	85	30	14.5	1.83		213.8	153.2	0.47	132.6	39.4
V	85	40	14.5	1.83		183.3	204.4	0.41	196.4	43.5
Ⅵ	90	0	14.5	1.83	65.6	323.4	0	0.57	66.4	25.3
Ⅶ	90	10	14.5	1.83		291.0	51.1	0.52	70.1	31.5
Ⅷ	90	20	14.5	1.83		258.7	102.2	0.46	100.2	37.2
Ⅸ	90	30	14.5	1.83		226.4	153.2	0.41	129.7	42.8
Ⅹ	90	40	14.5	1.83		194.0	204.4	0.37	162.7	45.3
Ⅺ	95	0	14.5	1.83	75.6	339.7	0	0.50	61.8	26.0
Ⅻ	95	10	14.5	1.83		305.7	51.1	0.45	81.3	33.0
XIII	95	20	14.5	1.83		271.7	102.2	0.41	110.4	40.7
XIV	95	30	14.5	1.83		237.8	153.2	0.37	132.8	46.9
XV	95	40	14.5	1.83		203.8	204.4	0.33	131.7	49.2

Note: D_{c} is the compaction degree of CDG; f_{v} is the volumetric content of IBA; $w_{\text{opt-C}}$, $S_{\text{r-C}}$, and $\rho_{\text{dmax-C}}$ are the optimum water content, degree of saturation, and maximum dry density for CDG, respectively; $m_{\text{s-C}}$ and $m_{\text{s-I}}$ are dry masses of CDG and IBA, respectively; e is the initial void ratio; and c_{ps} and φ_{ps} are the cohesion and internal friction angle at peak state, respectively

3 Testing results

Figs. 4-6 present photographs of the samples after the monotonic triaxial test. It can be observed that the IBA was distributed evenly in the samples, which confirmed the thoroughness of sample preparation. On the whole, the samples exhibited compression failure at a low f_{v} of IBA (such as 0%), without a distinct shear band. As f_{v} increased, more IBA was observed on the surfaces and the shear bands became more obvious. The effect of IBA, however, was difficult to discern visually.

Figs. 7-9 present the stress-strain curves of samples under different confining pressures, with the deviator stress q and volumetric strain ε_{v} plotted against the axial strain ε_{a}. The stresses in the legends represent the confining pressures (Figs. 7-9). For the variation of the volumetric strain, a negative value indicates dilatancy and a positive value indicates contraction (following Wang et al., 2018a). With a given confining pressure and compaction degree, the peak deviator stress $q_{\max}$ increases with the increase of f_{v}. Under the same confining pressure, the curve generally moves up with the increase of compaction degree, except for the case of $f_{\mathrm{v}}=40\%$. In general, samples exhibited contraction followed by dilatancy. With an increasing f_{v} value, the dilatancy became more pronounced. Under a given confining pressure, the effect of the compaction degree on the volumetric variation of the samples was not significant. For clarity, the initial/elastic modulus, cohesion, and internal friction angle at peak state, as well as the Poisson’s ratio and dilatancy angle, were also calculated for reference, as shown in Table 2.

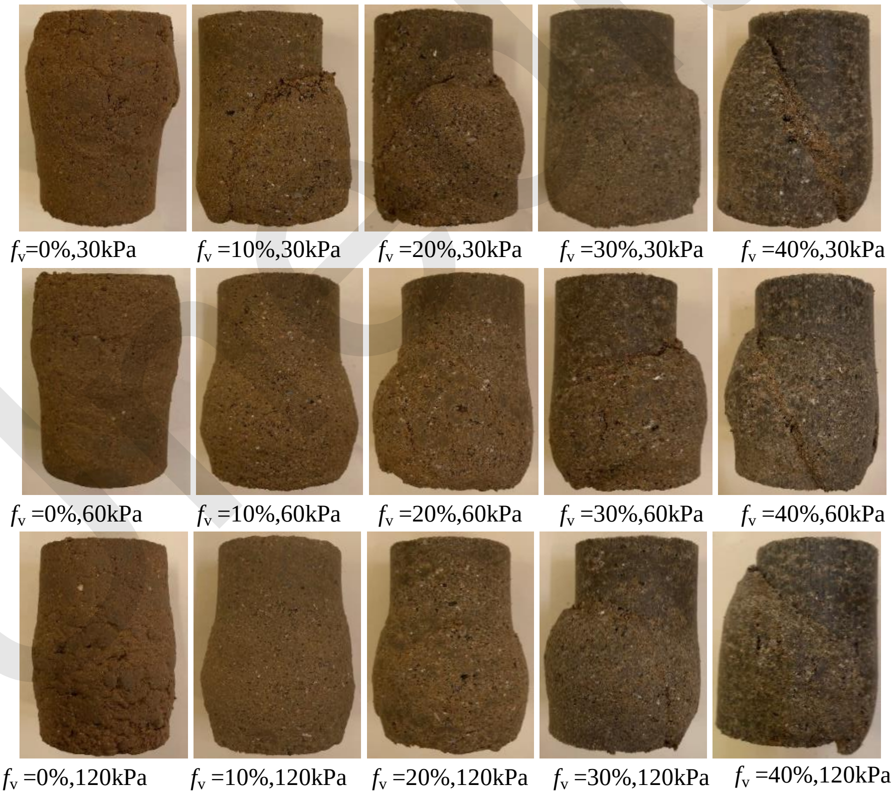
f_{v}=0%,30kPa f_{v} =10%,30kPa f_{v} =20%,30kPa f_{v} =30%,30kPa f_{v} =40%,30kPa

f_{v} =0%,60kPa f_{v} =10%,60kPa f_{v} =20%,60kPa f_{v} =30%,60kPa f_{v} =40%,60kPa

f_{v} =0%,120kPa f_{v} =10%,120kPa f_{v} =20%,120kPa f_{v} =30%,120kPa f_{v} =40%,120kPa

Fig. 4 Visual views of samples after shearing: D_{c} = 85%. Note: the stresses in this figure represent the confining pressures

Unedited

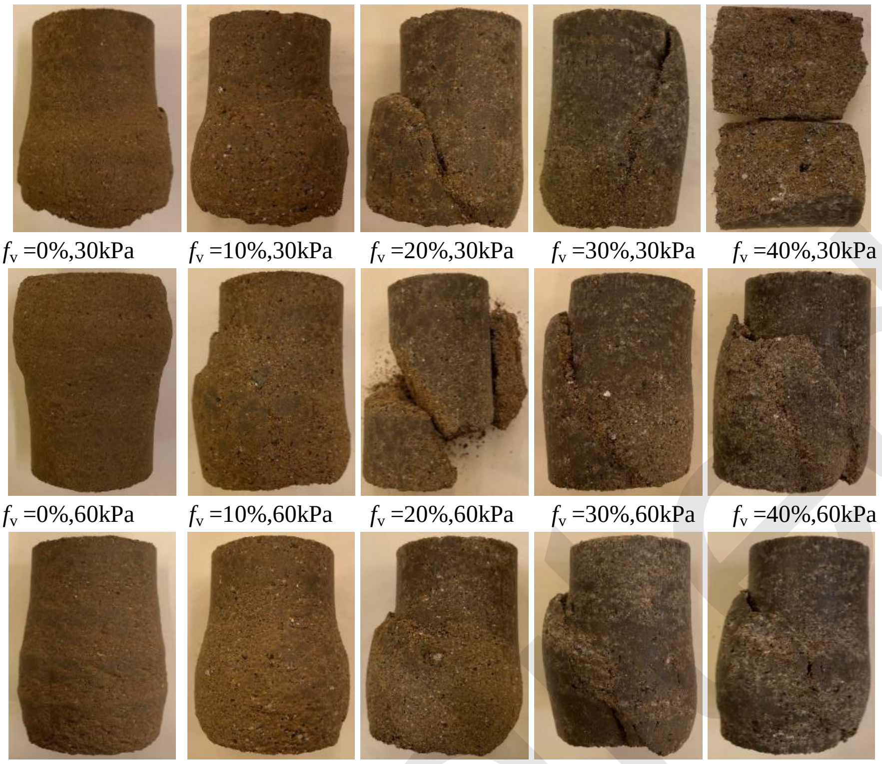

f_v =0%,30kPa f_v =10%,30kPa f_v =20%,30kPa f_v =30%,30kPa f_v =40%,30kPa

f_v =0%,60kPa f_v =10%,60kPa f_v =20%,60kPa f_v =30%,60kPa f_v =40%,60kPa

f_v =0%,120kPa f_v =10%,120kPa f_v =20%,120kPa f_v =30%,120kPa f_v =40%,120kPa

Fig. 5 Visual views of samples after shearing: D_c = 90%. Note: the stresses in this figure represent the confining pressures

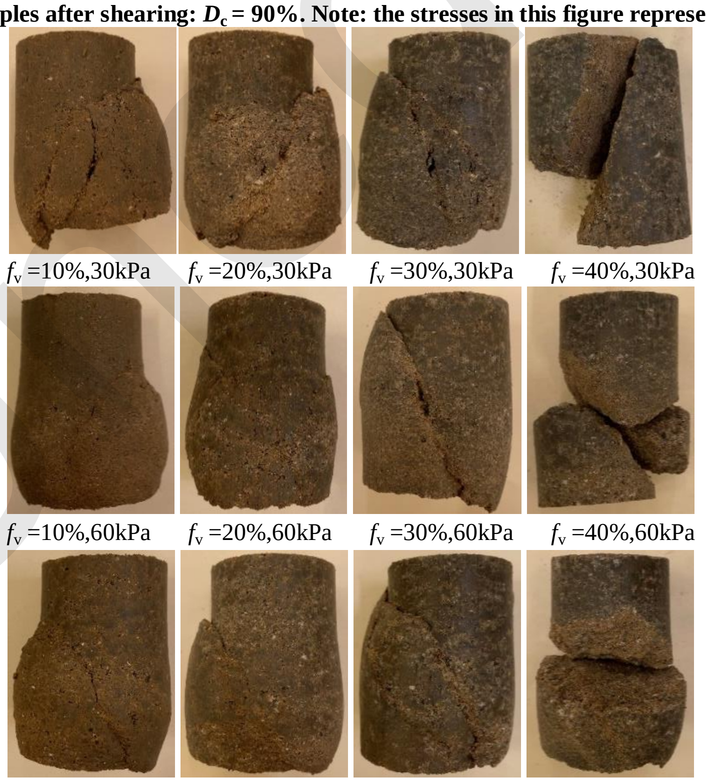

f_v =10%,30kPa f_v =20%,30kPa f_v =30%,30kPa f_v =40%,30kPa

f_v =10%,60kPa f_v =20%,60kPa f_v =30%,60kPa f_v =40%,60kPa

f_v =10%,120kPa f_v =20%,120kPa f_v =30%,120kPa f_v =40%,120kPa

Fig. 6 Visual views of samples after shearing: D_c = 95%. Note: the stresses in this figure represent the confining pressures

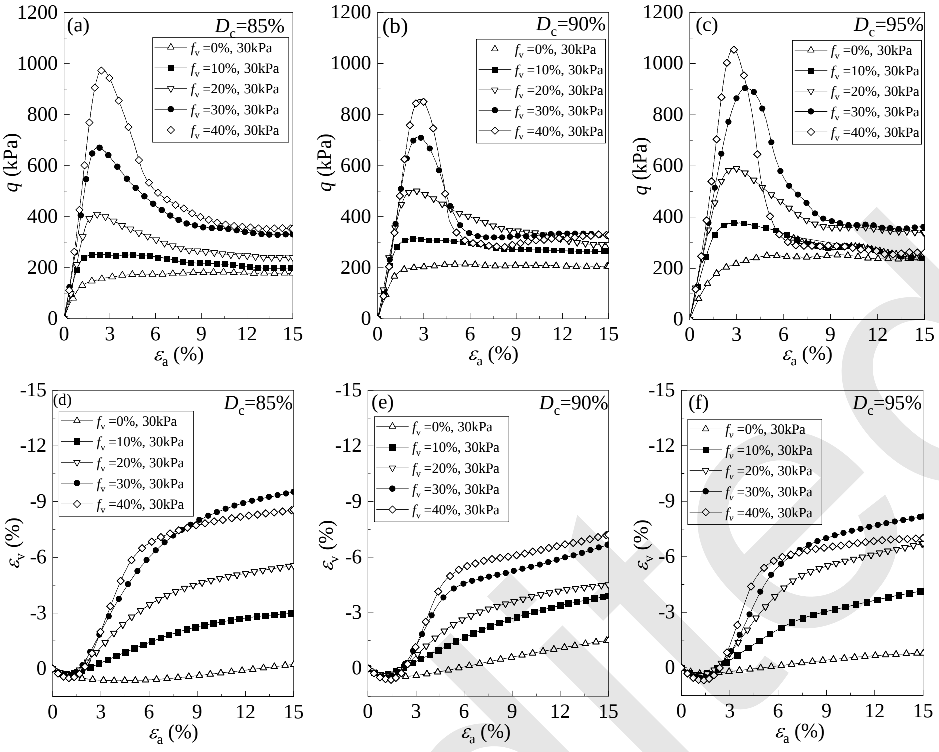

Fig. 7 Stress-strain behavior of all samples at σ_3 = 30 kPa: (a), (b), and (c) relationship between deviator stress and axial strain; (d), (e) and (f) relationship between volumetric strain and axial strain.

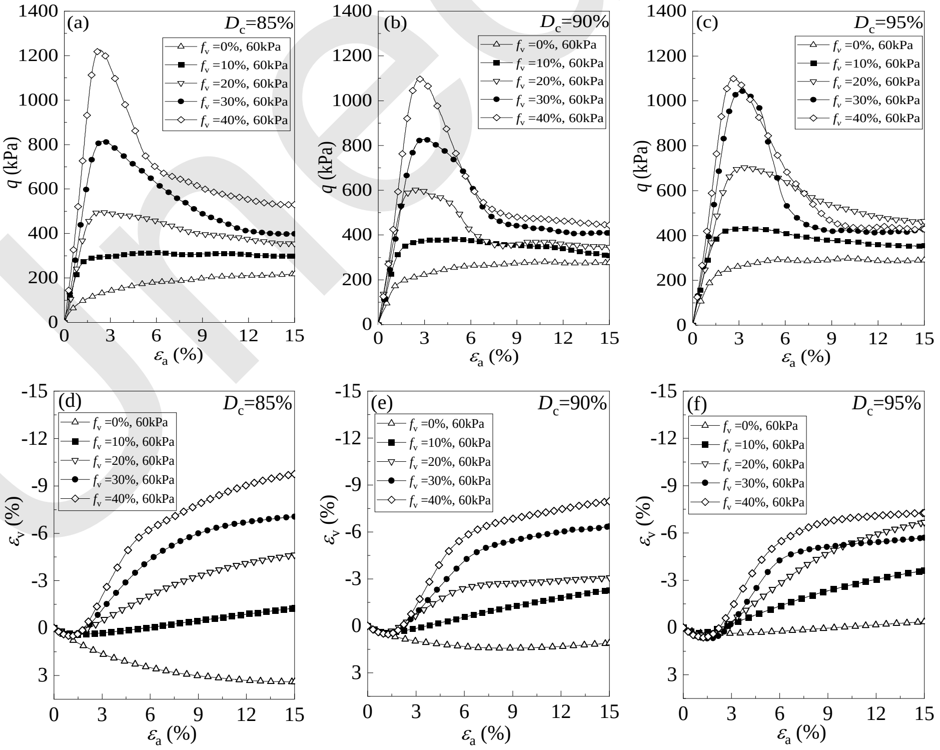

Fig. 8 Stress-strain behavior of all samples at σ_3 = 60 kPa: (a), (b), and (c) relationship between deviator stress and axial strain; (d), (e) and (f) relationship between volumetric strain and axial strain.

Unedited

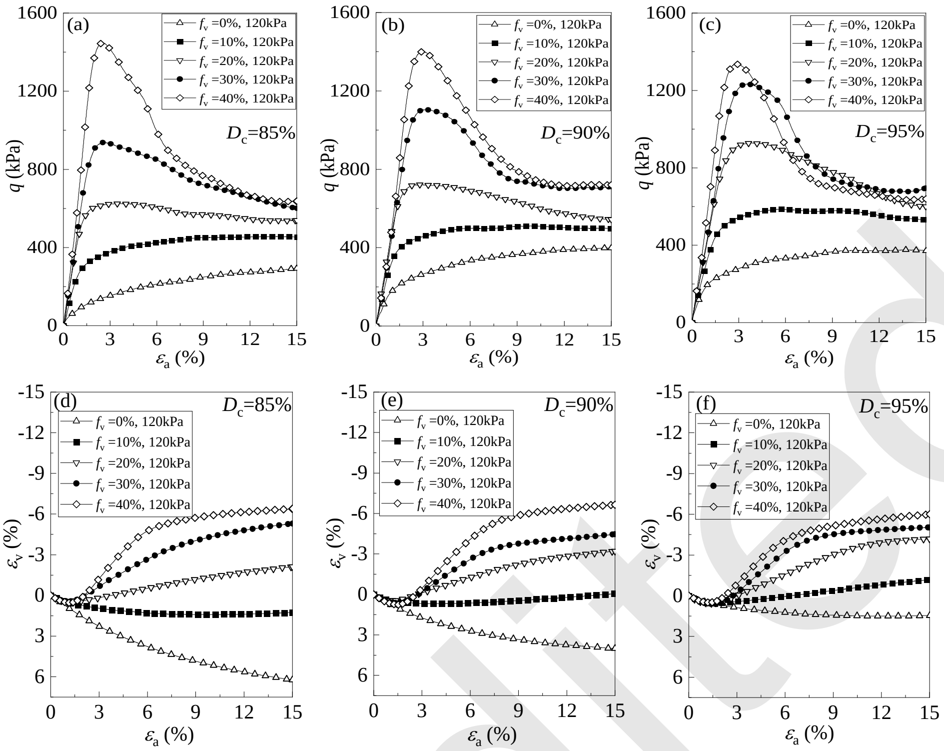

Fig. 9 Stress-strain behavior of all samples at σ_3 = 120 kPa: (a), (b), and (c) relationship between deviator stress and axial strain; (d), (e) and (f) relationship between volumetric strain and axial strain.

Unedited

4 Discussions

Fig. 10 shows the variation of the peak deviator stress $q_{\max}$ versus the volumetric content of IBA f_v, at different confining pressures and compaction degrees. At a specific compaction degree, we observe the bi-linear increasing trends of $q_{\max}$ with f_v. An intersection point can be identified by the two fitting lines with a given confining pressure and compaction degree. For all confining pressures, the intersection points fall in a narrow range for the volumetric content of IBA f_v, namely the characteristic volumetric content of IBA $f_{v\text{-cha}}$. In other words, at a given compaction degree, $q_{\max}$ increases slowly with the increase of f_v, before f_v reaches its characteristic value, regardless of the confining pressure. In this case, the CDG-CDG contacts control the mechanical behaviour of the samples. However, a dramatic increase of $q_{\max}$ appears with the increase of f_v beyond the characteristic value, with the CDG-IBA and IBA-IBA contacts dominating the mechanical behaviour. On the other hand, it is evident from Fig. 10 that as the compaction degree increases, the characteristic volumetric content of IBA $f_{v\text{-cha}}$ decreases. By analyzing the cross-section of the sample mixed with IBA and the triaxial testing results, this observation can be explained as follows.

Table 2 Mechanical properties of samples

Sample	D_c (%)	f_v (%)	σ_3 (kPa)	E_0 (MPa)	v	ψ (°)
I	85	0	30	17.0	0.18	2.8
	85	0	60	15.8	0.16	N.A.
	85	0	120	20.0	0.09	N.A.
II	85	10	30	23.9	0.20	12.7
	85	10	60	28.5	0.19	3.7
	85	10	120	30.1	0.17	N.A.
III	85	20	30	29.8	0.23	21.1
	85	20	60	30.1	0.18	12.9
	85	20	120	48.9	0.11	6.0
IV	85	30	30	38.4	0.18	27.4
	85	30	60	44.2	0.10	22.3
	85	30	120	55.9	0.12	16.1
V	85	40	30	39.8	0.14	32.4
	85	40	60	56.4	0.06	29.1
	85	40	120	65.7	0.14	24.2
Ⅵ	90	0	30	17.1	0.22	4.1
	90	0	60	17.3	0.20	N.A.
	90	0	120	25.0	0.17	N.A.
Ⅶ	90	10	30	25.1	0.20	10.3
	90	10	60	27.2	0.23	6.2
	90	10	120	34.0	0.18	2.7
Ⅷ	90	20	30	31.5	0.23	16.6
	90	20	60	37.0	0.10	15.5
	90	20	120	47.5	0.16	9.5
Ⅸ	90	30	30	38.1	0.17	26.7
	90	30	60	40.4	0.17	21.4
	90	30	120	53.2	0.13	17.0
Ⅹ	90	40	30	44.0	0.12	31.7
	90	40	60	55.3	0.11	24.5
	90	40	120	70.7	0.07	23.0
Ⅺ	95	0	30	15.3	0.32	2.8
	95	0	60	19.9	0.29	1.9
	95	0	120	23.9	0.24	N.A.
Ⅻ	95	10	30	24.4	0.19	12.7
	95	10	60	28.3	0.21	8.8
	95	10	120	30.4	0.18	3.5
XIII	95	20	30	28.9	0.15	21.1
	95	20	60	31.4	0.14	16.5
	95	20	120	43.3	0.11	12.1
XIV	95	30	30	36.8	0.14	27.4
	95	30	60	40.6	0.11	25.0
	95	30	120	50.6	0.09	19.7
XV	95	40	30	53.9	0.07	32.4
	95	40	60	54.2	0.07	27.3
	95	40	120	68.1	0.18	22.4

Note: D_c is the compaction degree of CDG; f_v is the volumetric content of IBA; σ_3 is the confining pressure; and E_0, v, and ψ are the initial/elastic modulus, Poisson's ratio, and dilatancy angle, respectively. N.A. = not applicable.

Unedited

Unedited

Fig. 11 plots the mechanism for the reinforcement of the CDG soil by the inclusion of IBA particles at two volumetric content levels. The coordination number N_{ci} is defined as the number of other particles closest to a single particle, to demonstrate the contacts of particles quantitatively. Taking the marked IBA particle enlarged in Fig. 11 as an example, the N_{ci} of this particle equals 2, 4, and 6. For the whole slice, the coordination number N_c is determined as the mean value of N_{ci} for all the inclusion particles (Patricia et al., 2006; Wang et al., 2018b):

$$N_c = \frac{\sum N_{ci}}{Q} \tag{6}$$

where N_{ci} = coordination number for each IBA particle; and Q = quantity of IBA particles in a slice.

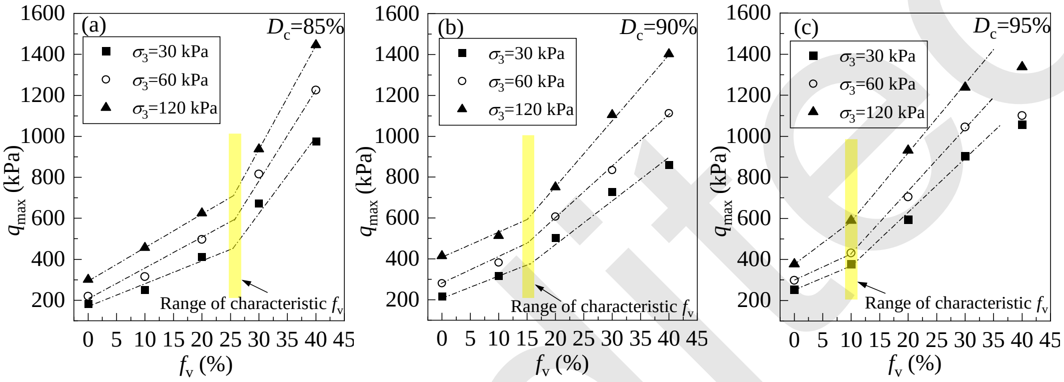

Fig. 10 Variations of peak deviator stress with f_v

When $f_v = f_{v1}$ and the compaction degree is 85%, 90%, and 95%, the coordination number N_c is approximately equal to 0.28, 0.37, and 0.48. As the volumetric content of IBA approaches f_{v2} ($f_{v2} < f_{v1}$), the coordination number N_c is approximately 0.19, 0.28, and 0.30 for the compaction degrees of 85%, 90%, and 95%. With greater compaction, the coordination number increases for a given volumetric content of IBA. At a given compaction degree, the coordination number also increases with the increase of volumetric content of IBA. The larger the coordination number, the larger the proportion of contact points of IBA. It can be seen from this example that the coordination number is the same for 85% compaction degree ($f_v = f_{v1}$) and 90% compaction degree ($f_v = f_{v2}$). This means that the same soil strength can be achieved by increasing either the compaction degree of the CDG or the volumetric content of IBA. In other words, increasing the compaction of the CDG can strengthen the controlling effect of the IBA contacts on the soil mechanical behaviour. This provides a direct verification that the characteristic volumetric content of IBA decreases with greater compaction of CDG soil (see Fig. 10).

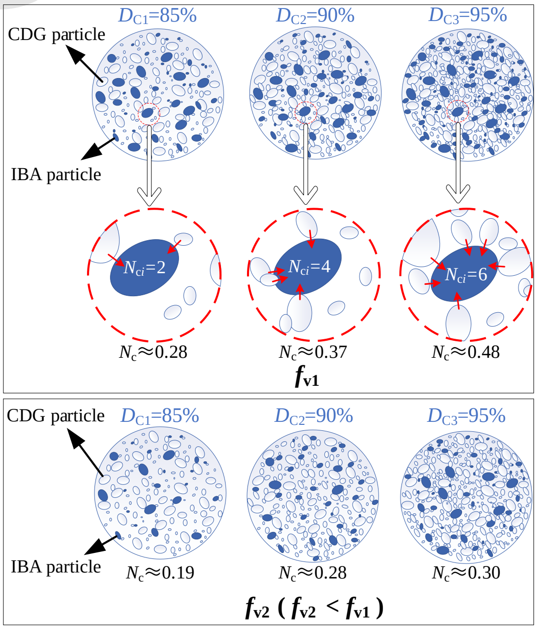

Fig. 11 Mechanism for reinforcement of CDG soil by the inclusion of IBA particles at two volumetric IBA contents

Unedited

5 Conclusions

In this study, we investigated the mechanical behaviour of a CDG-IBA mixture by performing a series of monotonic triaxial tests, with various volumetric contents of IBA and with different confining pressures and compaction degrees of the CDG soil. The CDG soil was kept in the same state for a given compaction degree, characterized by its optimum water content and designated dry density. Our findings, determined with the appropriate method, can serve as a reference for relevant studies on soil reinforcement using solid waste. The main conclusions are as follows.

(1) The test results show that adding more IBA particles leads to more significant dilatancy. Moreover, the maximum deviator stress increases with the volumetric content of IBA (a bi-linear increasing trend can be observed).

(2) Identification of the characteristic volumetric content of IBA allows the separation of two zones with different IBA effects. The higher the proportion of IBA contacts, the greater the influence on the soil and the stronger the shear strength. When the volumetric content of IBA is smaller than the characteristic value, the mechanical behaviour is dominated by CDG-CDG contacts. By contrast, when the volumetric content of IBA increases beyond the characteristic value, the CDG-IBA and IBA-IBA contacts become the dominant mechanism for the mechanical behaviour.

(3) As the compaction degree of the CDG increases, the coordination number of IBA increases, which strengthens the controlling effect of CDG-IBA and IBA-IBA contacts on the mechanical behaviour of the soil. As a result, the characteristic volumetric content of IBA decreases accordingly. In summary, similar soil reinforcement can be achieved by increasing either the compaction degree of the matrix soil or the inclusion content of IBA.

Acknowledgments

The financial supports from the National Natural Science Foundation of China (Grant Nos. 52378341, 51938005, 52090082) are gratefully acknowledged.

Author contributions

Han-Lin WANG, Zhen-Yu YIN, and Dong-Xing XUAN designed the research. Qian-Yi ZHANG and Cheng-Shuang YIN processed the corresponding data. Cheng-Shuang YIN wrote the first draft of the manuscript. Han-Lin WANG and Cheng-Shuang YIN helped to organize the manuscript. Han-Lin WANG, Cheng-Shuang YIN, and Qi-Wei LIU revised and edited the final version.

Conflict of interest

Han-Lin WANG, Cheng-Shuang YIN, Qian-Yi ZHANG, Qi-Wei LIU, Zhen-Yu YIN, and Dong-Xing XUAN declare that they have no conflict of interest.

References

Ahmed AT, Khalid HA, 2011. Effectiveness of novel and traditional treatments on the performance of incinerator bottom ash waste. Waste management, 31 (12): 2431-2439. https://doi.org/10.1016/j.wasman.2011.07.015

Alamanis N, Lokkas P, Chrysanidis TA, Christodoulou D, Paschalis E, 2021. Assessment principles for the mechanical behavior of clay soils. WSEAS Trans, 16: 47-61. https://doi.org/10.37394/232011.2021.16.6

Alhassan HM, Tankó AM, 2012. Characterization of solid waste incineration bottom ash and the potential for its use. International Journal of Engineering Research and Applications, 2(4): 516-522.

Anagnostopoulos CA, Chrysanidis T, Anagnostopoulou M, 2020. Experimental data of cement grouting in coarse soils with different superplasticisers. Data in Brief, 30: 105612. https://doi.org/10.1016/j.dib.2020.105612

ASTM (American Society for Testing and Materials), 2012. Standard test methods for laboratory compaction characteristics of soil using standard effort. ASTM D698-12. West Conshohocken, PA: ASTM International.

ASTM (American Society for Testing and Materials), 2017. Standard practice for classification of soils for engineering purposes (unified soil classification system). ASTM D2487-11. West Conshohocken, PA: ASTM International.

Chen RP, Qi S, Wang HL, Cui YJ, 2019. Microstructure and hydraulic properties of coarse-grained subgrade soil used in high-speed railway at various compaction degrees. Journal of Materials in Civil Engineering, 31(12): 04019301. https://doi.org/10.1061/(ASCE)MT.1943-5533.0002972

Dassekpo JBM, Zha X, Zhan J, 2017. Compressive strength performance of geopolymer paste derived from Completely Decomposed Granite (CDG) and partial fly ash replacement. Construction and Building Materials, 138: 195-203. https://doi.org/10.1016/j.conbuildmat.2017.01.133

Gruhler K, Bimesmeier T, Deilmann C, 2019. Secondary Materials in the Building Sector – Energy and Material Flows. IOP Conference Series: Earth and Environmental Science, 290(1): 012014.

Unedited

https://doi.org/10.1088/1755-1315/290/1/012014

Gupta G,Datta M, Ramana GV, Alappat BJ, 2021. MSW incineration bottom ash (MIBA) as a substitute to conventional materials in geotechnical applications: A characterization study from India and comparison with literature. Construction and Building Materials, 308: 124925. https://doi.org/10.1016/j.conbuildmat.2021.124925

Jiang X, Xiao R, Bai Y, Huang BS, Ma YT, 2022. Influence of waste glass powder as a supplementary cementitious material (SCM) on physical and mechanical properties of cement paste under high temperatures. Journal of Cleaner Production, 340: 130778. https://doi.org/10.1016/j.jclepro.2022.130778

Jiang X, Zhu HH, Yan ZG, Zhang FS, Ye F, Li P, Zhang XH, Dai ZR, Bai Y, Huang BS, 2023a. A state-of-art review on development and progress of backfill grouting materials for shield tunneling. Developments in the Built Environment, 100250. https://doi.org/10.1016/j.dibe.2023.100250

Jiang X, Zhang YY, Zhang Y, Ma JM, Xiao R, Guo FD, Bai Y, Huang BS, 2023b. Influence of size effect on the properties of slag and waste glass-based geopolymer paste. Journal of Cleaner Production, 383: 135428. https://doi.org/10.1016/j.jclepro.2022.135428

Lan HX, Hu RL, Yue ZQ, Lee CF, Wang SJ, 2003. Engineering and geological characteristics of granite weathering profiles in South China. Journal of Asian Earth Sciences, 21(4): 353-364. https://doi.org/10.1016/S1367-9120(02)00020-2

Lynn CJ, Ghataora GS, Obe RKD, 2017. Municipal incinerated bottom ash (MIBA) characteristics and potential for use in road pavements. International Journal of Pavement Research and Technology, 10(2): 185-201. https://doi.org/10.1016/j.ijprt.2016.12.003

Melese DT, 2022. Utilization of Waste Incineration Bottom Ash to Enhance Engineering Properties of Expansive Subgrade Soils. Advances in Civil Engineering, 2022: 7716921. https://doi.org/10.1155/2022/7716921

Patricia JC, Jean-Paul J, LANTUÉJOUL CHRISTIAN, 2006. Practical determination of the coordination number in granular media. Image Analysis & Stereology, 25(1): 55-61. https://doi.org/10.5566/ias.v25.p55-61

Randhawa KS, Chauhan R, 2022. Stabilizing black cotton soil in subgrade with municipal solid waste incineration ash for lowering greenhouse gas emission: A review. Materials Today: Proceedings, 50(P5): 1145-1151. https://doi.org/10.1016/j.matpr.2021.08.037

Seif El Dine B, Dupla JC, Frank R, Canou J, Kazan Y, 2010. Mechanical characterization of matrix coarse-grained soils with a large-sized triaxial device. Canadian Ge-otechnical Journal, 47(4): 425-438. https://doi.org/10.1139/T09-113

Tang P, Chen W, Xuan D, Zuo Y, and Poon C S, 2020. Investigation of cementitious properties of different constituents in municipal solid waste incineration bottom ash as supplementary cementitious materials. Journal of Cleaner Production, 258: 120675. https://doi.org/10.1016/j.jclepro.2020.120675

Toraldo E, Saponaro S, Careghini A, Mariani E, 2013. Use of stabilized bottom ash for bound layers of road pavements. Journal of Environmental Management, 121: 117-123. https://doi.org/10.1016/j.jenvman.2013.02.037

Wang HL, Cui YJ, Lamas-López F, Dupla JC, Canou J, Calon N, Saussine G, Aimedieu P, Chen RP, 2017. Effects of inclusion contents on resilient modulus and damping ratio of unsaturated track-bed materials. Canadian Geotechnical Journal, 54(12): 1672-1681. https://doi.org/10.1139/cgj-2016-0673

Wang HL, Cui YJ, Lamas-López F, Calon N, Saussine G, Dupla JC, Canou J, Aimedieu P, Chen RP, 2018a. Investigation on the mechanical behavior of track-bed materials at various contents of coarse grains. Construction and Building Materials, 164: 228-237. https://doi.org/10.1016/j.conbuildmat.2017.12.209

Wang HL, Cui YJ, Lamas-López F, Dupla JC, Canou J, Calon N, Saussine G, Aimedieu P, Chen RP, 2018b. Permanent Deformation of Track-Bed Materials at Various Inclusion Contents under Large Number of Loading Cycles. Journal of Geotechnical and Geoenvironmental Engineering, 144(8): 04018044. https://doi.org/10.1061/(ASCE)GT.1943-5606.0001911

Wang HL, Pathak B, Yin ZY, 2023. Investigation on microstructure, unconfined compressive strength, and thermal conductivity of compacted CDG soil by MICP treatment during curing. Journal of Materials in Civil Engineering, 35(6): 04023131. https://doi.org/10.1061/JMCEE7.MTENG-14901

Xuan D, Tang P, Poon CS, 2018. Limitations and quality upgrading techniques for utilization of MSW incineration bottom ash in engineering applications – A review. Construction and Building Materials, 190: 1091-1102. https://doi.org/10.1016/j.conbuildmat.2018.09.174

Xu W, Yin ZY, Wang HL, Wang X, 2022. Experimental study on the monotonic mechanical behavior of completely decomposed granite soil reinforced by disposable face-mask chips. Journal of Cleaner Production, 352: 131528. https://doi.org/10.1016/j.jclepro.2022.131528

中文概要

题　目：不同焚烧残渣掺量下压实全风化花岗岩加固土静力学特性

作　者：王瀚霖[1,2,3], 尹承双[1,2,3], 张谦益[4], 刘骐炜[1,2,3], 尹振宇[5]; 玄东兴[5]

机　构：[1]湖南大学，地下空间开发先进技术研究中心，中国长沙，410082；[2]湖南大学，建筑安全与节能教育部重点实验室，中国长沙，410082；[3]湖南大学，土木工程学院，中国长沙，410082；[4]郑州大学，土木工程学院，中国郑州，450001；[5]香港理工大学，土木与环境工程系，中国香港，九龙，红磡

摘　要：近年来，生活垃圾不断增加，产生了大量的焚烧残渣(IBA)。同时，考虑到土建材料的巨大用量需求和有限的自然资源，充分利用固废材料变得越来越重要。本研究通过静三轴试验，研究了不同IBA体积含量和不同CDG压实度下IBA对压实全分化花岗岩(CDG)试样静力学特性的影响。结果表明，随着IBA体积含量的增加，最大偏应力或抗剪强度逐渐增大，呈双线性增加趋势。当IBA的体积含量超过某一特征值时，增长速率更加显著。到达此值之前，CDG-CDG接触主导力学特性，而在达到此值之后，CDG-IBA和IBA-IBA接触为主导。且随着压实度的增加，由于IBA配位数和IBA接触比例增加，IBA的特征体积含量值降低。因此，在实际工程中，无论是提高CDG的压实度还是提高IBA的体积含量，都有助于提高加固土体的目标强度。

关键词：全风化花岗岩；焚烧残渣；压实度；特征体积含量；土体加固

Unedited